Propulsion and Power Research 2016;5(2):134–148

HOSTED BY

ELSEVIER

http://ppr.buaa.edu.cn/

Propulsion and Power Research

www.sciencedirect.com

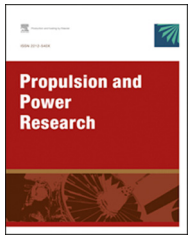

ORIGINAL ARTICLE

MHD flow of a nanofluid in an expanding or contracting porous pipe with chemical reaction and heat source/sink

S. Srinivas[a,*], **A. Vijayalakshmi**[a], **A. Subramanyam Reddy**[a], **T.R. Ramamohan**[b]

[a]*Department of Mathematics, School of Advanced Sciences, VIT University, Vellore 632014, India*
[b]*CSIR Fourth Paradigm Institute (Formerly, CSIR Center for Mathematical Modeling and Computer Simulation), Wind Tunnel Road, Bangalore 560037, India*

Received 30 December 2014; accepted 1 June 2015
Available online 26 May 2016

KEYWORDS

Porous pipe;
Chemical reaction parameter;
Brownian motion parameter;
Thermophoresis parameter;
Lewis number

Abstract In the present investigation, an analytical analysis has been carried out to study the influence of chemical reaction on MHD flow of a nanofluid in an expanding or contracting porous pipe in the presence of heat source/sink. The pipe wall expands or contracts uniformly at a time dependent rate. Similarity transformations have been invoked to reduce the governing flow equations into coupled nonlinear ordinary differential equations. An analytical approach, namely the homotopy analysis method (HAM) is employed to obtain the analytical solutions of the ordinary differential equations. The convergence of the obtained series solutions is analyzed. The effects of various physical parameters such as wall expansion ratio, Brownian motion parameter, thermophoresis parameter, Lewis number, chemical reaction parameter and heat source/sink parameter on flow variables have been discussed. Further, for the case of hydrodynamic viscous fluid, we find a good agreement between the HAM solutions and solutions already reported in the literature.

1. Introduction

In recent years, study of laminar flow in a porous pipe or channel with expanding or contracting walls received much attention of several researchers due to their wide

*Corresponding author. Tel.: +91 416 2202514; fax: +91 416 2243092.
E-mail address: srinusuripeddi@hotmail.com (S. Srinivas).

Peer review under responsibility of National Laboratory for Aeronautics and Astronautics, China.

http://dx.doi.org/10.1016/j.jppr.2016.04.004

Nomenclature

$a(t)$	radius of the pipe
$\dot{a}(t)$	time dependent rate
A	the injection/suction coefficient
B_0	applied magnetic field
C	dimensional nanoparticle concentration
C_0	reference nanoparticle concentration at the center
C_p	specific heat at constant pressure (unit: J/(kg·K))
C_w	nanoparticle concentration at the wall
k_1	first order chemical reaction rate
K_1	dimensionless constant
Le	Lewis number
M	Hartmann number
Nt	thermophoresis parameter
Nb	Brownian motion parameter
$\hat{p}$	dimensional pressure (unit: Pa)
Pr	Prandtl number
Q	heat source/sink parameter
R	permeation Reynolds number
$\hat{r}, \hat{z}$	dimensional cylindrical coordinates (unit: m)
T	dimensional temperature (unit: K)
T_0	reference temperature at the center
T_m	mean temperature
T_w	temperature at the wall
$\hat{u}, \hat{v}$	velocity components along $\hat{r}$ and $\hat{z}$ directions respectively (unit: m/s)
v_w	injection/suction velocity
Q_0	dimensional heat source/sink

Greek symbols

ρ_f	density of the base fluid (unit: kg/m^3)
σ	electrical conductivity (unit: S/m)
β	thermal diffusivity (unit: m^2/s)
η	dimensionless radial position
α	dimensionless wall expansion ratio
μ	dynamic viscosity of the fluid (unit: N·s/m^2)
ν	kinematic viscosity of the fluid (unit: m^2/s)
γ	dimensionless chemical reaction parameter
$(\rho C_p)_p$	heat capacity of the nanoparticle (unit: kg/(m^3·K))
$(\rho C_p)_f$	heat capacity of the fluid (unit: kg/(m^3·K))
θ	dimensionless temperature
$\hat{\psi}$	stream function (unit: m^2/s)
ψ	dimensionless stream function
τ	ratio between the heat capacity of the nanoparticle and heat capacity of the fluid
ϕ	dimensionless nanoparticles concentration

Subscripts

f	base fluid
p	nanoparticle
w	pipe wall

applications in technological as well as biological flows. For example, in the transport of biological fluids through expanding or contracting vessels, the synchronous pulsation of porous diaphragms, the air circulation in the respiratory system and the regression of the burning surface in solid rocket motors [1–8]. Boutros et al. [9] have applied Lie-group method for unsteady flows in a semi-infinite expanding or contracting pipe with injection or suction through a porous wall. Si et al. [10] have analyzed the problem of laminar flow in a porous pipe with suction at slowly expanding or contracting wall. Asghar et al. [11] analyzed the flow in a slowly deforming channel with weak permeability. Srinivas et al. [12] studied the thermal diffusion and diffusion thermo effects in a two-dimensional viscous flow between slowly expanding or contracting walls with weak permeability. Recently, Srinivas et al. [13] have investigated the influence of heat transfer on MHD flow in a pipe with expanding or contracting permeable wall by employing homotopy analysis method (HAM).

Nanofluid is a liquid containing nanometer-sized particles having diameter less than 100 nm, called nanoparticle [14]. Nanoparticle is currently an area of intense scientific interest due to a wide range of applications in biomedical, optical and electronic field. These can be found in metals such as (Al, Cu), oxides (Al_2O_3), carbides (SiC), nitrides (AlN, SiN) or nanometals (Graphite, carbon-nanotubes) [15–20]. Buongiorno [21] examined the convective heat transport in nanofluids. In this study the author developed a two-component four equation nonhomogeneous equilibrium models for mass momentum and heat transport in nanofluids. Further, Buongiorno [21] concluded that in the absence of turbulent effects, the Brownian diffusion and thermophoresis will be important and also he has considered the conservation equations based on these two effects. Rosca and Pop [22] have examined unsteady boundary layer flow of a nanofluid past a moving surface in an external uniform free stream using Buongiorno's model. The natural convective boundary layer flow of nanofluid over a flat vertical plate was investigated by Kuznetsov and Nield [23]. Nadeem et al. [24] have studied non-orthogonal stagnation point flow of a non-Newtonian fluid towards a stretching surface with heat transfer. Xu and Pop [25] examined the fully developed mixed convection flow in vertical channel filled with nanofluids. Mustafa et al. [26] investigated MHD boundary layer flow of second grade nanofluid over a stretching sheet with convective boundary conditions by employing HAM. Alsaedi et al. [27] applied HAM to study the effect of heat generation/absorption on stagnation point flow of nanofluid over a surface with convective boundary conditions. Chamkha et al. [28] analyzed the free convective boundary layer flow of a nanofluid over a vertical cylinder. Malvandi et al. [29] used modified Buongiorno's model for fully developed mixed convection flow of nanofluid in a vertical annular pipe. Fully developed mixed convection in horizontal and inclined tubes with uniform heat flux using nanofluid was

considered by Akbari et al. [30]. Ellahi [31] obtained analytical solutions to study the effects of MHD and temperature dependent viscosity on the flow of non-Newtonian nanofluid in a pipe by employing HAM. Uddin et al. [32] developed a model of bio-nano-materials processing to the hydromagnetic transport phenomena from a stretching or shrinking nonlinear nanomaterial sheet with Navier slip and convective heating. Xu et al. [33] discussed the problem of fully developed mixed convective flow of a nanofluid in a vertical channel using Buongiorno mathematical model. Malik et al. [34] studied the boundary layer flow and heat transfer of a Casson nanofluid over a vertical exponentially stretching cylinder. Malvandi and Ganji [35] analyzed the Brownian motion and thermophoresis effects on slip flow of alumina/water nanofluid inside a circular micro channel in the presence of a magnetic field. Zaimi et al. [36] obtained numerical solutions for unsteady flow and heat transfer of a nanofluid over a contracting cylinder by using shooting method. Recently, Srinivas et al. [37] have analyzed the hydromagnetic flow of a nanofluid in a porous channel with expanding or contracting walls by using HAM. Most recently, Hedayati and Ganji [38] have investigated the effects of nanoparticle migration and mixed convection of titania/water nanofluid inside a vertical micro channel. Malvandi et al. [39] have studied the MHD mixed convection of alumina/water nanofluid inside a vertical annular pipe.

It is well known that chemical reaction effect plays a vital role in the study of heat and mass transfer in many branches of science and engineering. Possible applications of this type of flow can be found in many industries and engineering applications such as nuclear reactor safety, combustion systems, solar collectors, metallurgy, and chemical engineering. Some investigations have been carried out in this direction by several researchers [40–42]. Nadeem and Akbar [43] have examined the influence of heat and chemical reactions on Walter's B fluid model for blood flow through a tapered artery. Hayat and Abbas [44] have studied the channel flow of a Maxwell fluid with chemical reaction. Abdul-Kahar et al. [45] analyzed chemical reaction and heat radiation effects on boundary-layer flow of a nanofluid past a porous vertical stretching surface by using scaling group transformation. Kameswaran et al. [46] have investigated the effects of homogeneous–heterogeneous reaction in nanofluid flow over a porous stretching sheet. A numerical analysis of magnetoconvective boundary layer slip flow along a non-isothermal continuously moving permeable nonlinear radiating plate in Darcian porous media with chemical reaction have investigated by Uddin et al. [47]. Rashidi et al. [48] employed optimal homotopy analysis method (OHAM) to study the free convective flow of a nanofluid past a chemically reacting horizontal plate in porous media. Recently, Srinivas et al. [49] have analyzed the mass transfer effects on viscous flow in an expanding or contracting porous pipe with chemical reaction. Most recently, Uddin et al. [50] studied the magnetohydrodynamic free convective boundary layer flow of a chemically reacting nanofluid from a convectively heated permeable vertical surface.

A literature survey reveals that no attempt regarding the influence of chemical reaction on MHD flow of a nanofluid in an expanding or contracting porous pipe in the presence of heat source/sink has been made so far. Such a consideration is of great value in biological and engineering research. Keeping this in view, the main aim of the present work is to investigate the effects of chemical reaction on MHD flow of a nanofluid in an expanding or contracting porous pipe in presence of heat source/sink. The governing flow equations are transformed into a system of coupled nonlinear ordinary differential equations by using similarity transformations and then solved analytically by using homotopy analysis method (HAM) proposed by Liao [51]. It is worth mentioning that HAM has been applied successfully to many interesting problems [13,20,31,44,52–57]. The features of the flow characteristics are analyzed by plotting graphs and discussed in detail. The organization of the paper is as follows: the problem is formulated in Section 2. Section 3 includes the solution procedure of the problem. Numerical results and discussion are given in Section 4 and the conclusions have been summarized in Section 5.

2. Formulation of the problem

Consider the laminar and incompressible electrically conducting nanofluid flow in an expanding or contracting porous pipe of a semi-infinite length. The radius of the pipe is $a(t)$. The wall has equal permeability and expands or contracts uniformly at a time dependent rate $\dot{a}(t)$. A magnetic field of uniform strength B_0 is applied perpendicular to the wall. As shown in Figure 1, a coordinate system can be chosen with the origin at the center of the pipe. Take the $\hat{z}$ coordinate axis parallel to the pipe wall and the $\hat{r}$ coordinate axis perpendicular to the wall. Under these assumptions the governing equations are [1,2,9,10,21,22,28,29,33,34,36,45]

$$\frac{\partial \hat{u}}{\partial \hat{z}} + \frac{\partial \hat{v}}{\partial \hat{r}} + \frac{\hat{v}}{\hat{r}} = 0 \tag{1}$$

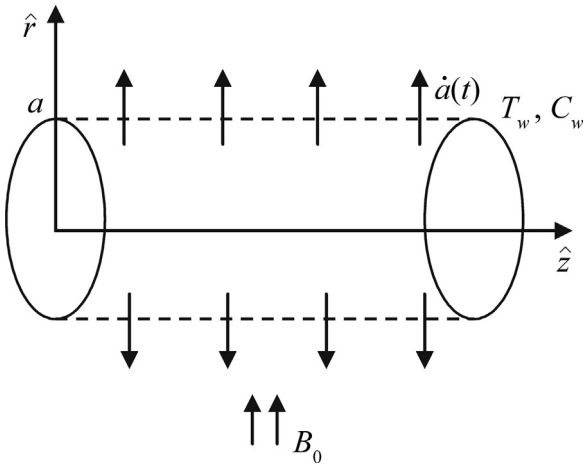

Figure 1 Porous pipe with expanding or contracting wall.

$$\frac{\partial \hat{u}}{\partial t}+\hat{u}\frac{\partial \hat{u}}{\partial \hat{z}}+\hat{v}\frac{\partial \hat{u}}{\partial \hat{r}}=-\frac{1}{\rho_f}\frac{\partial \hat{p}}{\partial \hat{z}} +\nu\left[\frac{\partial^2 \hat{u}}{\partial \hat{r}^2}+\frac{1}{\hat{r}}\frac{\partial \hat{u}}{\partial \hat{r}}+\frac{\partial^2 \hat{u}}{\partial \hat{z}^2}\right]-\frac{\sigma B_0^2}{\rho_f}\hat{u} \tag{2}$$

$$\frac{\partial \hat{v}}{\partial t}+\hat{v}\frac{\partial \hat{v}}{\partial \hat{z}}+\hat{v}\frac{\partial \hat{v}}{\partial \hat{r}}=-\frac{1}{\rho_f}\frac{\partial \hat{p}}{\partial \hat{r}} +\nu\left[\frac{\partial^2 \hat{v}}{\partial \hat{r}^2}+\frac{1}{\hat{r}}\frac{\partial \hat{v}}{\partial \hat{r}}+\frac{\partial^2 \hat{v}}{\partial \hat{z}^2}-\frac{\hat{v}}{\hat{r}^2}\right] \tag{3}$$

$$\frac{\partial T}{\partial t}+\hat{u}\frac{\partial T}{\partial \hat{z}}+\hat{v}\frac{\partial T}{\partial \hat{r}}=\beta\left(\frac{\partial^2 T}{\partial \hat{r}^2}+\frac{1}{\hat{r}}\frac{\partial T}{\partial \hat{r}}+\frac{\partial^2 T}{\partial \hat{z}^2}\right) +\tau\left[D_B\left(\frac{\partial C}{\partial \hat{r}}\frac{\partial T}{\partial \hat{r}}+\frac{\partial C}{\partial \hat{z}}\frac{\partial T}{\partial \hat{z}}\right) +\frac{D_T}{T_m}\left\{\left(\frac{\partial T}{\partial \hat{r}}\right)^2+\left(\frac{\partial T}{\partial \hat{z}}\right)^2\right\}\right] +\frac{Q_0}{(\rho C_p)_f}(T-T_0) \tag{4}$$

$$\frac{\partial C}{\partial t}+\hat{u}\frac{\partial C}{\partial \hat{z}}+\hat{v}\frac{\partial C}{\partial \hat{r}}=D_B\left(\frac{\partial^2 C}{\partial \hat{r}^2}+\frac{1}{\hat{r}}\frac{\partial C}{\partial \hat{r}}+\frac{\partial^2 C}{\partial \hat{z}^2}\right) +\frac{D_T}{T_m}\left\{\frac{\partial^2 T}{\partial \hat{r}^2}+\frac{1}{\hat{r}}\frac{\partial T}{\partial \hat{r}}+\frac{\partial^2 T}{\partial \hat{z}^2}\right\}-k_1 C \tag{5}$$

where $\hat{u}$, $\hat{v}$ are the components of velocity along the $\hat{z}$ and $\hat{r}$ directions respectively, ρ_f is the fluid density, $\hat{p}$ is dimensional pressure, t is time, ν is kinematic viscosity, σ is electrical conductivity, B_0 is the strength of applied magnetic field, C_p is specific heat at constant pressure, β is thermal diffusivity, T_m is the mean temperature, D_B is Brownian diffusion coefficient, D_T is thermophoretic diffusion coefficient, k_1 is the first order chemical reaction rate ($k_1>0$ for destructive reaction, $k_1=0$ for no reaction, $k_1<0$ for generative reaction), T and C are temperature and nanoparticles concentration and $\tau=\frac{(\rho C_p)_p}{(\rho C_p)_f}$.

The corresponding boundary conditions are

$$\hat{u}=0,\quad \hat{v}=-v_w=-A\dot{a},\qquad T=T_w,\quad C=C_w,\quad \text{at } \hat{r}=a(t) \tag{6}$$

$$\frac{\partial \hat{u}}{\partial \hat{r}}=0,\quad \hat{v}=0,\quad \frac{\partial T}{\partial \hat{r}}=0,\quad \frac{\partial C}{\partial \hat{r}}=0 \text{ at } \hat{r}=0 \tag{7}$$

$$\hat{u}=0,\quad \hat{v}=0 \quad \text{at} \quad \hat{z}=0. \tag{8}$$

The injection/suction coefficient A that appears in Eq. (6) is the measure of wall permeability and T_w, C_w are the temperature and nanoparticle concentration at wall.

Introduce a stream function which satisfies the continuity Eq. (1)

$$\hat{\psi}=\nu\hat{z}F(\eta,t) \tag{9}$$

where $\eta=\frac{\hat{r}}{a}$ is the dimensionless radial position.

The axial and radial velocity components can be written as

$$\hat{u}=\frac{1}{\hat{r}}\frac{\partial \psi}{\partial \hat{r}}=\frac{\nu\hat{z}\hat{F}_\eta(\eta,t)}{a^2\eta},\qquad \hat{v}=-\frac{1}{\hat{r}}\frac{\partial \psi}{\partial \hat{z}}=-\frac{\nu\hat{F}(\eta,t)}{a\eta} \tag{10}$$

Substituting the Eq. (10) in the Eqs. (2) and (3) and then eliminating pressure, one can obtain

$$\eta^2\hat{F}_{\eta\eta\eta\eta}+(\alpha\eta^3-2\eta)\hat{F}_{\eta\eta\eta}+(\alpha\eta^2+3)\hat{F}_{\eta\eta} -\left(\alpha\eta+\frac{3}{\eta}\right)\hat{F}_\eta+\hat{F}_\eta^2-\eta\hat{F}_\eta\hat{F}_{\eta\eta}+\eta\hat{F}\hat{F}_{\eta\eta\eta}-3\hat{F}\hat{F}_{\eta\eta} +\frac{3}{\eta}\hat{F}\hat{F}_\eta-M^2(\eta^2\hat{F}_{\eta\eta}-\eta\hat{F}_\eta)-\frac{a^2}{\nu}\left(\frac{\hat{F}}{\eta}\right)_{\eta t}\eta^3=0. \tag{11}$$

where $\alpha=\frac{a\dot{a}}{\nu}$ is the non-dimensional wall dilation rate and is defined to be positive for expansion and negative for contraction and $M=\frac{\sqrt{\sigma}B_0 a}{\sqrt{\mu}}$ is the Hartmann number and μ is dynamic viscosity.

The corresponding boundary conditions given by Eqs. (6)–(8) transform into

$$\hat{F}(0,t)=0,\quad \hat{F}(1,t)=R,\quad \hat{F}_\eta(1,t)=0,\qquad \lim_{\eta\to 0}\frac{\partial}{\partial\eta}\left(\frac{1}{\eta}\frac{\partial \hat{F}(\eta,t)}{\partial\eta}\right)=0 \tag{12}$$

where R is the permeation Reynolds number and is defined by $R=\frac{av_w}{\nu}=A\alpha$. Note that R is positive for injection and negative for suction. A similar solution with respect to both space and time can be developed by following the transformation described by Uchida and Aoki [1] and Majdalani and Zhou [3] independently. For constant α and $\hat{F}=\hat{F}(\eta)$, it follows that $\left(\frac{\hat{F}_\eta}{\eta}\right)_{\eta t}=0$. To realize this condition, the value of the expansion ratio α must be specified by the initial value

$$\alpha=\frac{a\dot{a}}{\nu}=\frac{a_0\dot{a}_0}{\nu}=\text{constant} \quad \text{or} \quad \frac{\dot{a}_0}{\dot{a}}=\frac{a}{a_0} \tag{13}$$

where a_0 and $\dot{a}_0$ denote the initial radius and expansion rate. Forthwith, the temporal similarity transformation can be achieved by integrating Eq. (13) with respect to time. The result is

$$\frac{a}{a_0}=\sqrt{1+2\nu\alpha t a_0^{-2}}. \tag{14}$$

Since $v_w=A\dot{a}$, an expression for the injection velocity can be determined, proved that the injection coefficient A is constant. From Eqs. (13) and (14), it is clear that

$$\frac{\dot{a}_0}{\dot{a}} = \frac{v_w(0)}{v_w(t)} = \sqrt{1 + 2\nu\alpha t a_0^{-2}}. \tag{15}$$

Under these provisions Eq. (11) becomes

$$\eta^3\hat{F}''' + \alpha(\eta^4\hat{F}'''' + \eta^3\hat{F}''' - \eta^2\hat{F}') - 2\eta^2\hat{F}''' + 3\eta\hat{F}'' - 3\hat{F}' + \eta\hat{F}'^2 - 3\eta\hat{F}\hat{F}'' + 3\hat{F}\hat{F}' + 3\eta^2\hat{F}\hat{F}''' - \eta^2\hat{F}'\hat{F}'' - M^2(\eta^3\hat{F}'' - \eta^2\hat{F}') = 0. \tag{16}$$

The corresponding boundary conditions are

$$\hat{F}(0) = 0, \quad \hat{F}'(1) = 0, \quad \hat{F}(1) = R, \quad \lim_{\eta\to 0}\left(\frac{\hat{F}'}{\eta}\right)' = 0\,. \tag{17}$$

Eqs. (10), (16) and (17) can be normalized by putting

$$\psi = \frac{\hat{\psi}}{a\dot{a}}, \quad u = \frac{\hat{u}}{\dot{a}}, \quad v = \frac{\hat{v}}{\dot{a}}, \quad z = \frac{\hat{z}}{a}, \quad f = \frac{\hat{F}}{R} \tag{18}$$

and so

$$\eta^3 f''' + \alpha(\eta^4 f'''' + \eta^3 f''' - \eta^2 f') - 2\eta^2 f''' + 3\eta f'' - 3f' + \eta R f'^2 - 3\eta R f f'' + 3R f f' + 3\eta^2 R f f'''' - \eta^2 f' f'' - M^2(\eta^3 f'' - \eta^2 f') = 0 \tag{19}$$

$$f(0) = 0, \quad f'(1) = 0, \quad f(1) = 1, \quad \lim_{\eta\to 0}\left(\frac{f'}{\eta}\right)' = 0. \tag{20}$$

It may be noted that when $\alpha = 0$ and $M = 0$, Eq. (19) is the case that Majdalani and Flandro [5] have described.

The temperature of the fluid and the nanoparticles concentration in the pipe can be expressed as

$$T = T_0 + (T_w - T_0)\theta(\eta), \quad C = C_0 + (C_w - C_0)\phi(\eta) \tag{21}$$

where T_0, C_0 are the reference temperature and nanoparticle concentration at the center.

The dimensionless forms of temperature and nanoparticle concentration from Eq. (21) are

$$\theta = \frac{T - T_0}{T_w - T_0}, \quad \phi = \frac{C - C_0}{C_w - C_0}. \tag{22}$$

Substituting Eq. (21) into Eqs. (4) and (5), one obtains

$$\eta\theta'' + \alpha Pr\eta^2\theta' + RPrf\theta' + Nb\eta\theta'\phi' + Nt\eta\theta'^2 + \theta' + QPr\eta\theta = 0 \tag{23}$$

$$\eta\phi'' + \alpha LePr\eta^2\phi' + RLePrf\phi' + \eta\frac{Nt}{Nb}\theta'' + \frac{Nt}{Nb}\theta' + \phi' - \gamma LePr\eta\phi - LePrK_1\eta = 0 \tag{24}$$

with the boundary conditions

$$\theta'(0) = 0, \quad \theta(1) = 1, \quad \phi'(0) = 0, \quad \phi(1) = 1. \tag{25}$$

where $Pr = \frac{\nu}{\beta}$ is Prandtl number, $Nb = \frac{\tau D_B(C_w - C_0)}{\beta}$ is the Brownian motion parameter, $Nt = \frac{\tau D_T(T_w - T_0)}{T_m\beta}$ is thermophoresis parameter, $Le = \frac{\beta}{D_B}$ is Lewis number, $Q = \frac{Q_0 a^2}{(\rho C_p)_f \nu}$ is heat source/sink parameter (i.e., positive for heat source and negative for heat sink), $\gamma = \frac{k_1 a^2}{\nu}$ is the chemical reaction parameter which is positive for destructive chemical reaction and negative for generative reaction and $K_1 = \frac{k_1 C_0 a^2}{\nu(C_w - C_0)}$.

3. Solution of the problem

To develop analytical solutions by HAM as a polynomial base function, the boundary conditions in Eq. (20) become:

$$f(0) = 0, \quad f(1) = 1, \quad f'(1) = 0, \quad f'(0) = 0. \tag{26}$$

For the HAM solutions of Eqs. (19), (23) and (24), the initial approximations f_0, θ_0 and ϕ_0 and auxiliary linear operators L_1, L_2 and L_3 are as follows:

$$f_0(\eta) = 3\eta^2 - 2\eta^3, \quad \theta_0(\eta) = 1, \quad \phi_0(\eta) = 1 \tag{27}$$

$$L_1(f) = \frac{d^4 f}{d\eta^4}, \quad L_2(\theta) = \frac{d^2\theta}{d\eta^2}, \quad L_3(\phi) = \frac{d^2\phi}{d\eta^2} \tag{28}$$

with

$$L_1\left(c_1\eta^3 + c_2\eta^2 + c_3\eta + c_4\right) = 0, \quad L_2(c_5\eta + c_6) = 0, \quad L_3(c_7\eta + c_8) = 0 \tag{29}$$

where $c_i (i = 1-8)$ are constants.

3.1. Zero-order deformation equations

Let $p \in [0, 1]$ be an embedding parameter and h be the auxiliary non-zero parameter. The deformation equations at zero-order can be written as follows:

$$(1-p)L_1\left[\hat{f}(\eta;p) - f_0(\eta)\right] = ph_f N_1\left[\hat{f}(\eta;p)\right] \tag{30}$$

$$\hat{f}(0;p) = 0, \quad \hat{f}(1;p) = 1, \quad \hat{f}'(1;p) = 0, \quad \hat{f}'(0;p) = 0 \tag{31}$$

$$(1-p)L_2\left[\hat{\theta}(\eta;p) - \theta_0(\eta)\right] = ph_\theta N_2\left[\hat{\theta}(\eta;p), \hat{f}(\eta;p), \hat{\phi}(\eta;p)\right] \tag{32}$$

$$\hat{\theta}(1;p) = 1, \quad \hat{\theta}'(0;p) = 0 \tag{33}$$

$$(1-p)L_3\left[\hat{\phi}(\eta;p)-\phi_0(\eta)\right]=ph_\phi N_3\left[\hat{\phi}(\eta;p),\hat{f}(\eta;p),\hat{\theta}(\eta;p)\right] \tag{34}$$

$$\hat{\phi}(1;p)=1,\quad \hat{\phi}'(0;p)=0 \tag{35}$$

where

$$\begin{aligned}N_1\left[\hat{f}(\eta;p)\right]&=\eta^3\frac{\partial^4\hat{f}(\eta;p)}{\partial\eta^4}+\alpha\left[\eta^4\frac{\partial^3\hat{f}(n;p)}{\partial\eta^3}\right.\\&\left.+\eta^3\frac{\partial^2\hat{f}(n;p)}{\partial\eta^2}-\eta^2\frac{\partial\hat{f}(n;p)}{\partial\eta}\right]-2\eta^2\frac{\partial^3\hat{f}(n;p)}{\partial\eta^3}\\&+3\eta\frac{\partial^2\hat{f}(n;p)}{\partial\eta^2}-3\frac{\partial\hat{f}(n;p)}{\partial\eta}+R\eta\left[\frac{\partial\hat{f}(n;p)}{\partial\eta}\right]^2\\&-R\eta^2\frac{\partial\hat{f}(n;q)}{\partial\eta}\frac{\partial^2\hat{f}(n;p)}{\partial\eta^2}-3R\eta\hat{f}(\eta;p)\frac{\partial^2\hat{f}(\eta;p)}{\partial\eta^2}\\&+3R\eta\hat{f}(\eta;q)\frac{\partial\hat{f}(\eta;p)}{\partial\eta}+R\eta^2\hat{f}(\eta;q)\frac{\partial^3\hat{f}(\eta;p)}{\partial\eta^3}\\&-M^2\left[\eta^3\frac{\partial^2\hat{f}(\eta;p)}{\partial\eta^2}-\eta^2\frac{\partial\hat{f}(\eta;p)}{\partial\eta}\right]\end{aligned} \tag{36}$$

$$\begin{aligned}N_2\left[\hat{\theta}(\eta;p),\hat{f}(\eta;p),\hat{\phi}(\eta;p)\right]&=\eta\frac{\partial^2\hat{\theta}(\eta;p)}{\partial\eta^2}\\&+\alpha Pr\eta^2\frac{\partial\hat{\theta}(\eta;p)}{\partial\eta}+RPr\hat{f}(\eta;p)\frac{\partial\hat{\theta}(\eta;p)}{\partial\eta}\\&+Nb\eta\frac{\partial\hat{\theta}(\eta;p)}{\partial\eta}\frac{\partial\hat{\phi}(\eta;p)}{\partial\eta}+Nt\eta\left(\frac{\partial\hat{\theta}(\eta;p)}{\partial\eta}\right)^2\\&+\frac{\partial\hat{\theta}(\eta;p)}{\partial\eta}+QPr\eta\hat{\theta}(\eta;p)\end{aligned} \tag{37}$$

$$\begin{aligned}N_3\left[\hat{\phi}(\eta;p),\hat{f}(\eta;p),\hat{\theta}(\eta;p)\right]&=\eta\frac{\partial^2\hat{\phi}(\eta;p)}{\partial\eta^2}+\alpha LePr\eta^2\\&\frac{\partial\hat{\phi}(\eta;p)}{\partial\eta}+RLePr\hat{f}(\eta;p)\frac{\partial\hat{\phi}(\eta;p)}{\partial\eta}+\eta\frac{Nt}{Nb}\frac{\partial^2\hat{\theta}(\eta;p)}{\partial\eta^2}\\&+\frac{Nt}{Nb}\frac{\partial\hat{\theta}(\eta;p)}{\partial\eta}+\frac{\partial\hat{\phi}(\eta;p)}{\partial\eta}-\gamma LePr\eta\hat{\phi}(\eta;p)-K_1LePr\eta.\end{aligned} \tag{38}$$

For $p=0$ and $p=1$, we have

$$\begin{aligned}&\hat{f}(\eta;0)=f_0(\eta),\ \ \hat{f}(\eta;1)=f(\eta),\\&\hat{\theta}(\eta;0)=\theta_0(\eta),\ \ \hat{\theta}(\eta;1)=\theta(\eta),\\&\hat{\phi}(\eta;0)=\phi_0(\eta),\ \ \hat{\phi}(\eta;1)=\phi(\eta).\end{aligned} \tag{39}$$

Further, by Taylor's series expansion, one obtains

$$\hat{f}(\eta)=f_0(\eta)+\sum_{m=1}^{\infty}f_m(\eta)p^m \tag{40}$$

where $f_m(\eta)=\left.\frac{1}{m!}\frac{\partial^m\hat{f}(\eta;p)}{\partial p^m}\right|_{p=0}$

$$\hat{\theta}(\eta)=\theta_0(\eta)+\sum_{m=1}^{\infty}\theta_m(\eta)p^m \tag{41}$$

where $\theta_m(\eta)=\left.\frac{1}{m!}\frac{\partial^m\hat{\theta}(\eta;p)}{\partial p^m}\right|_{p=0}$

$$\hat{\phi}(\eta)=\phi_0(\eta)+\sum_{m=1}^{\infty}\phi_m(\eta)p^m \tag{42}$$

where $\phi_m(\eta)=\left.\frac{1}{m!}\frac{\partial^m\hat{\phi}(\eta;p)}{\partial p^m}\right|_{p=0}$.

We choose h_f, h_θ and h_ϕ, properly in such a way that these series are convergent at $p=1$, therefore we have the solution expressions from Eqs. (40)–(42) as follows:

$$f(\eta)=f_0(\eta)+\sum_{m=1}^{\infty}f_m(\eta) \tag{43}$$

$$\theta(\eta)=\theta_0(\eta)+\sum_{m=1}^{\infty}\theta_m(\eta) \tag{44}$$

$$\phi(\eta)=\phi_0(\eta)+\sum_{m=1}^{\infty}\phi_m(\eta). \tag{45}$$

3.2. The high-order deformation equations

Differentiating the zero-order deformation Eqs. (30)–(35) m times with respect to p, then dividing by $m!$ and finally setting $p=0$, one obtains the following mth order deformation equations:

$$L_1\left[f_m(\eta)-\chi_m f_{m-1}(\eta)\right]=h_f R_{1,m}(\eta) \tag{46}$$

$$L_2\left[\theta_m(\eta)-\chi_m\theta_{m-1}(\eta)\right]=h_\theta R_{2,m}(\eta) \tag{47}$$

$$L_3\left[\phi_m(\eta)-\chi_m\phi_{m-1}(\eta)\right]=h_\phi R_{3,m}(\eta) \tag{48}$$

where

$$\begin{aligned}R_{1,m}&=\eta f''''_{m-1}+\alpha\left[\eta^4 f''_{m-1}+\eta^3 f''_{m-1}-\eta^2 f'_{m-1}\right]\\&-2\eta^2 f'''_{m-1}+3\eta f''_{m-1}-3f'_{m-1}+R\eta\sum_{k=0}^{m-1}f'_{m-1-k}f'_k\\&-R\eta^2\sum_{k=0}^{m-1}f'_{m-1-k}f''_k-3R\eta\sum_{k=0}^{m-1}f_{m-1-k}f''_k\\&+3R\sum_{k=0}^{m-1}f_{m-1-k}f'_k+R\eta^2\sum_{k=0}^{m-1}f_{m-1-k}f'''_k\\&-M^2\left[\eta^3 f''_{m-1}-\eta^2 f'_{m-1}\right]\end{aligned} \tag{49}$$

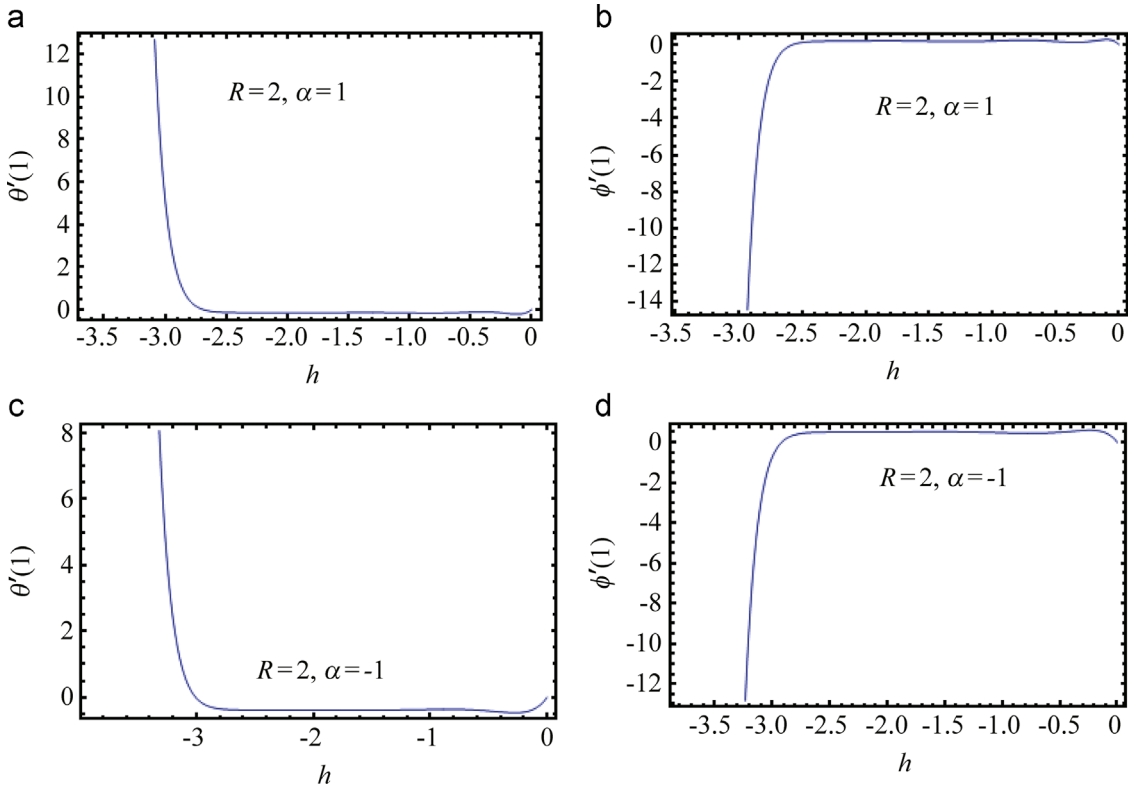

Figure 2 h-curves for the 20th order approximations for the functions θ, ϕ for $M=2$, $Pr=7$, $Nb=Nt=0.2$, $Le=1.25$, $Q=0.5$, $\gamma=0.5$, $K_1=0.1$.

$$R_{2,m}=\eta\theta''_{m-1}+\alpha Pr\eta^2\theta'_{m-1}+RPr\sum_{k=0}^{m-1}f_{m-1-k}\theta'_k+Nb\eta\sum_{k=0}^{m-1}\theta'_{m-1-k}\phi'_k+Nt\eta\sum_{k=0}^{m-1}\theta'_{m-1-k}\theta'_k+\theta'_{m-1}+QPr\eta\theta_{m-1} \tag{50}$$

$$R_{3,m}=\eta\phi''_{m-1}+\alpha LePr\eta^2\phi'_{m-1}+RLePr\sum_{k=0}^{m-1}f_{m-1-k}\phi'_k+\frac{Nt}{Nb}\eta\theta''_{m-1}+\frac{Nt}{Nb}\theta'_{m-1}+\phi'_{m-1}-\gamma LePr\eta\phi_{m-1}-K_1LePr\eta(1-\chi_m) \tag{51}$$

and

$$\chi_m=\begin{cases}1, & m\neq 1\\ 0, & m=1\end{cases}. \tag{52}$$

The corresponding boundary conditions are

$$f_m(0)=f_m(1)=f'_m(1)=f'_m(0)=0 \tag{53}$$

$$\theta_m(1)=\theta'_m(0)=0,\qquad \phi_m(1)=\phi'_m(0)=0. \tag{54}$$

To solve Eqs. (46)–(48) with the conditions Eqs. (52)–(54), we use the symbolic computation software MATHEMATICA.

Table 1 The 20th order approximation for the optimal convergence-control parameter h and corresponding square residual error (SRE) for $R=2$, $\alpha=1$, $M=2$, $Pr=7$, $Q=0.5$, $\gamma=0.5$, $Nb=Nt=0.2$, $Le=1.25$, $K_1=0.1$.

h	SRE of f	SRE of θ	SRE of ϕ
−0.7	8.49337×10^{-2}	2.26237×10^{-3}	8.34136×10^{-3}
−0.8	5.70298×10^{-2}	1.87724×10^{-3}	7.97921×10^{-3}
−0.9	4.02977×10^{-2}	1.51339×10^{-3}	6.84244×10^{-3}
−1	2.96384×10^{-2}	1.14937×10^{-3}	5.52003×10^{-3}
−1.1	2.25109×10^{-2}	8.74954×10^{-4}	4.68229×10^{-3}
−1.2	1.75532×10^{-2}	7.01274×10^{-4}	4.26881×10^{-3}
−1.25	1.56315×10^{-2}	6.37454×10^{-4}	4.08721×10^{-3}
−1.30	1.39902×10^{-2}	5.80984×10^{-4}	3.86788×10^{-3}
−1.35	1.25789×10^{-2}	5.28484×10^{-4}	3.60132×10^{-3}
−1.40	1.13591×10^{-2}	4.78725×10^{-4}	3.30084×10^{-3}
−1.45	1.02958×10^{-2}	4.3192×10^{-4}	2.99259×10^{-3}
−1.50	9.36762×10^{-3}	3.88914×10^{-4}	2.70408×10^{-3}
−1.55	8.57398×10^{-3}	3.50409×10^{-4}	2.45504×10^{-3}
−1.60	7.86291×10^{-3}	3.16704×10^{-4}	2.25316×10^{-3}
−1.65	7.19241×10^{-3}	2.87607×10^{-4}	2.09425×10^{-3}
−1.70	6.8687×10^{-3}	2.62538×10^{-4}	1.96674×10^{-3}
−1.75	1.11932×10^{-2}	2.4078×10^{-4}	1.85472×10^{-3}
−1.80	2.04833×10^{-2}	2.21541×10^{-4}	1.7472×10^{-3}

3.3. Convergence of HAM solution

The convergence of the series solutions and rate of convergence for the HAM depend upon the convergence-control

parameter h. If h is properly chosen, the homotopy series solution may converge rapidly. Hence to compute the range of admissible values of h_θ and h_ϕ, the h-curves plotted in Figure 2. The range of admissible values of h_θ and h_ϕ are $-2.6 \le h_\theta \le -0.4$ and $-2.5 \le h_\phi \le -0.2$ respectively. Further, we define the square residual error to prove the correctness of the h-curves. Substituting the approximate solutions of $f(\eta)$, $\theta(\eta)$ and $\phi(\eta)$ obtain by HAM into Eqs. (19), (23) and (24) yields the residual error as follows:

$$E_1 = \eta^3 f''' + \alpha(\eta^4 f'''' + \eta^3 f'' - \eta^2 f) - 2\eta^2 f''' + 3\eta f'' - 3f' + \eta R f'^2 - 3\eta R f f'' + 3R f f' + 3\eta^2 R f f''' - \eta^2 f' f'' - M^2(\eta^3 f'' - \eta^2 f') \quad (55)$$

$$E_2 = \eta\theta'' + \alpha Pr\eta^2\theta' + RPrf\theta' + Nb\eta\theta'\phi' + Nt\eta\theta'^2 + \theta' + QPr\eta\theta \quad (56)$$

Table 2 The 20th order approximation for the optimal convergence-control parameter h and corresponding square residual error (SRE) $R = 2$, $\alpha = -1$, $M = 2$, $Pr = 7$, $Q = 0.5$, $\gamma = 0.5$, $Nb = Nt = 0.2$, $Le = 1.25$, $K_1 = 0.1$.

h	SRE of f	SRE of θ	SRE of ϕ
−0.8	6.36048×10^{-2}	1.74009×10^{-3}	3.85152×10^{-3}
−0.9	3.89656×10^{-2}	1.40645×10^{-3}	3.39659×10^{-3}
−1	2.56252×10^{-2}	1.13797×10^{-3}	2.92321×10^{-3}
−1.1	1.78083×10^{-2}	9.32050×10^{-4}	2.50986×10^{-3}
−1.2	1.29252×10^{-2}	7.81285×10^{-4}	2.1640×10^{-3}
−1.25	1.11607×10^{-2}	7.22231×10^{-4}	2.07478×10^{-3}
−1.30	9.71200×10^{-3}	6.71444×10^{-4}	1.9787×10^{-3}
−1.35	8.51124×10^{-3}	6.27139×10^{-4}	1.87944×10^{-3}
−1.40	7.50617×10^{-3}	5.87817×10^{-4}	1.79561×10^{-3}
−1.45	6.66067×10^{-3}	5.5231×10^{-4}	1.71544×10^{-3}
−1.50	5.93838×10^{-3}	5.19768×10^{-4}	1.63616×10^{-3}
−1.55	5.32191×10^{-3}	4.89614×10^{-4}	1.55629×10^{-3}
−1.60	4.78207×10^{-3}	4.61491×10^{-4}	1.47538×10^{-3}
−1.65	4.33502×10^{-3}	4.35187×10^{-4}	1.39385×10^{-3}
−1.70	3.90952×10^{-3}	4.10584×10^{-4}	1.31259×10^{-3}
−1.75	3.67279×10^{-3}	3.87613×10^{-4}	1.23275×10^{-3}
−1.80	3.25586×10^{-3}	3.66259×10^{-4}	1.15545×10^{-3}
−1.85	4.54801×10^{-3}	3.46445×10^{-4}	1.08166×10^{-3}

$$E_3 = \eta\phi'' + \alpha LePr\eta^2\phi' + RLePrf\phi' + \eta\frac{Nt}{Nb}\theta'' + \frac{Nt}{Nb}\theta' + \phi' - \gamma LePr\eta\phi - LePrK_1\eta \quad (57)$$

where E_1, E_2 and E_3 correspond to the residual error for $f(\eta)$, $\theta(\eta)$ and $\phi(\eta)$ respectively. We show the square residual error (SRE) for $f(\eta)$, $\theta(\eta)$ and $\phi(\eta)$ in Tables 1 and 2. From these tables it can be seen that the different values of h lead to minimum average square residual error for $f(\eta)$, $\theta(\eta)$ and $\phi(\eta)$. Also Figure 3 is plotted to show the SRE for $f(\eta)$, $\theta(\eta)$ and $\phi(\eta)$ for $\alpha = 1$ and $\alpha = -1$. In order to check the analytical solution, we compare the results corresponding to the radial velocity with that of Boutros et al. (Ref. [9]) in Tables 3 and 4 for the case of hydrodynamic viscous fluid. It is clear that the present

Table 3 Radial velocity observations in the case of suction for different values of α for the hydrodynamic viscous fluid: $M = 0$, $R = -100$.

α	η	$\frac{v}{A}$ (Boutros et al. [9])	$\frac{v}{A}$ HAM (20th order)	$\frac{v}{A}$ HAM (25th order)
50	0.91652	−1.039776	−1.03641	−1.03942
20	0.88318	−1.053519	−1.05519	−1.05628
0	0.86023	−1.06745	−1.06842	−1.06864
−5	0.86023	−1.07158	−1.07151	−1.07157
−10	0.84853	−1.07626	−1.07492	−1.07491

Table 4 Radial velocity observations in the case of suction for different values of α for the hydrodynamic viscous fluid: $M = 0$, $R = -1000$.

α	η	$\frac{v}{A}$ (Boutros et al. [9])	$\frac{v}{A}$ HAM (20th order)	$\frac{v}{A}$ HAM (25th order)
50	0.87178	−1.06298	−1.06527	−1.06506
20	0.86023	−1.06528	−1.06736	−1.06714
0	0.86023	−1.06693	−1.06859	−1.06838
−5	0.86023	−1.06734	−1.06889	−1.06868
−10	0.86023	−1.06776	−1.06919	−1.06899

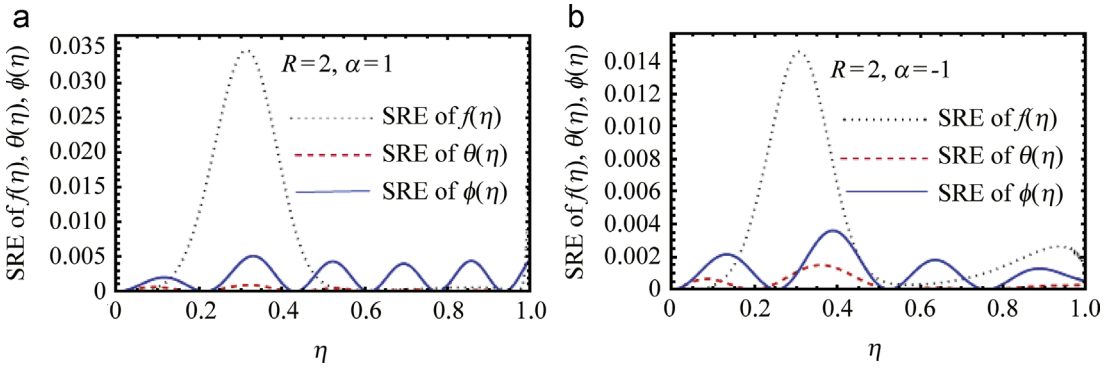

Figure 3 Square residual error (SRE) of f, θ, ϕ for $M = 2$, $Pr = 7$, $Nb = Nt = 0.2$, $Le = 1.25$, $Q = 0.5$, $\gamma = 0.5$, $K_1 = 0.1$.

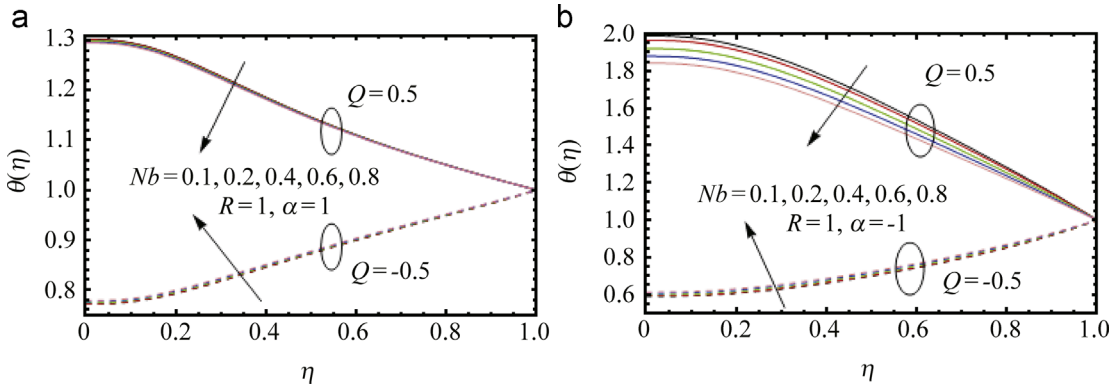

Figure 4 Effect of Brownian motion parameter *Nb* on temperature distribution.

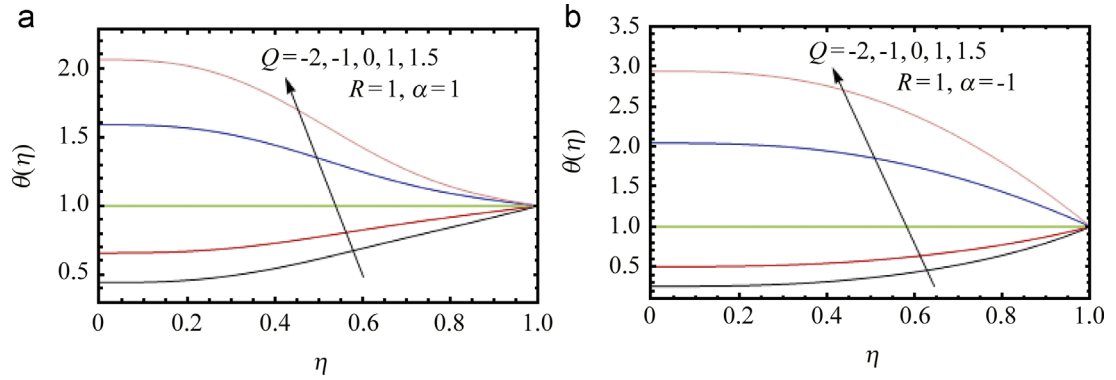

Figure 5 Effect of heat source parameter *Q* on temperature distribution.

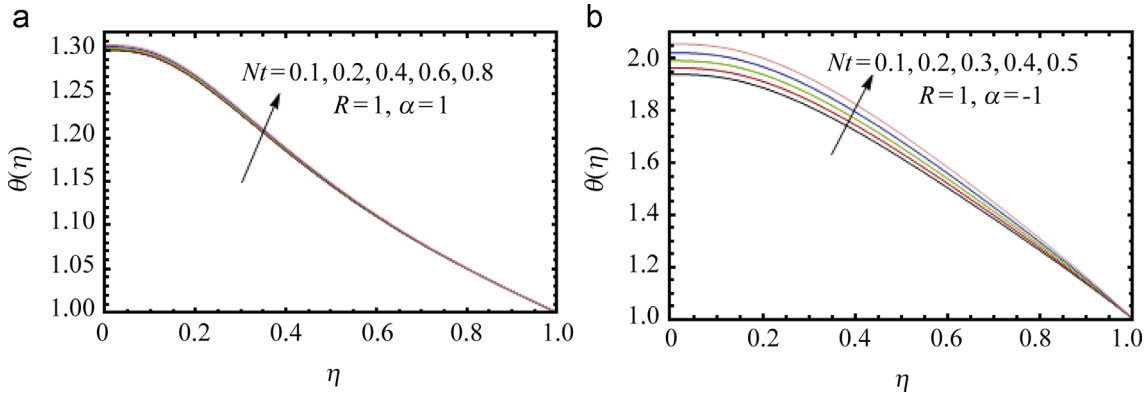

Figure 6 Effect of thermophoresis parameter *Nt* on temperature distribution.

results are in good agreement with the results of Boutros et al. [9]. Further, the heat and mass transfer rates in terms of the dimensionless form of Nusselt number and Sherwood number at the wall are defined as

$$Nu = -\theta'(\eta)_{\eta=1},$$
$$Sh = -\phi'(\eta)_{\eta=1}. \quad (58)$$

4. Results and discussion

This section describes the influence of various physical parameters that have been emerged in the mathematical formulation on the dimensionless temperature, nanoparticle concentration, Nusselt number and Sherwood number distributions by assigning numerical values and the results are shown graphically in Figures 4–17. Special emphasis has been given to Brownian motion parameter *Nb*, heat source/sink parameter *Q*, thermophoresis parameter *Nt*, the wall expansion ratio α, Hartmann number *M*, Prandtl number *Pr* and the permeation Reynolds number *R*, chemical reaction parameter γ and Lewis number *Le*. To understand the physics of the problem, we choose $Pr = 7$, $Nb = Nt = 0.2$, $Le = 5$, $Q = 0.5$, $\gamma = 0.5$, $M = 2$ and $K_1 = 0.1$ unless otherwise stated. It may be noted that the

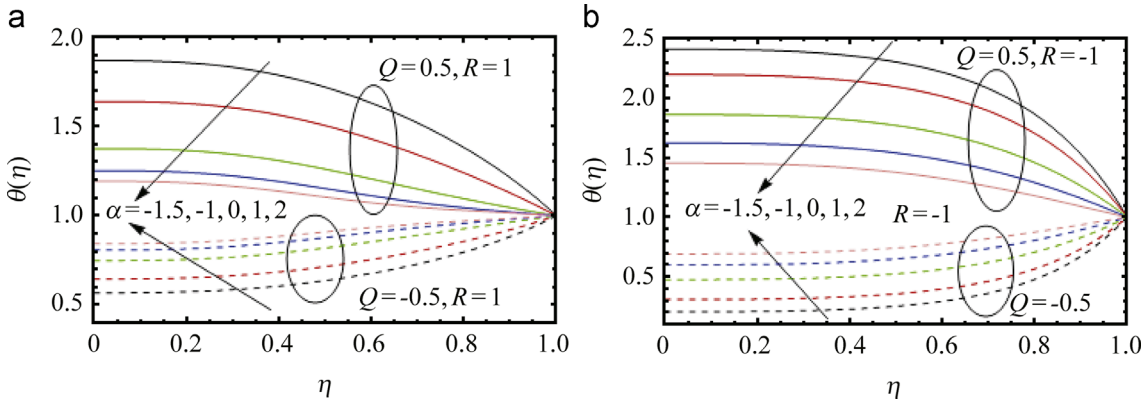

Figure 7 Effect of wall expansion ratio α on temperature distribution.

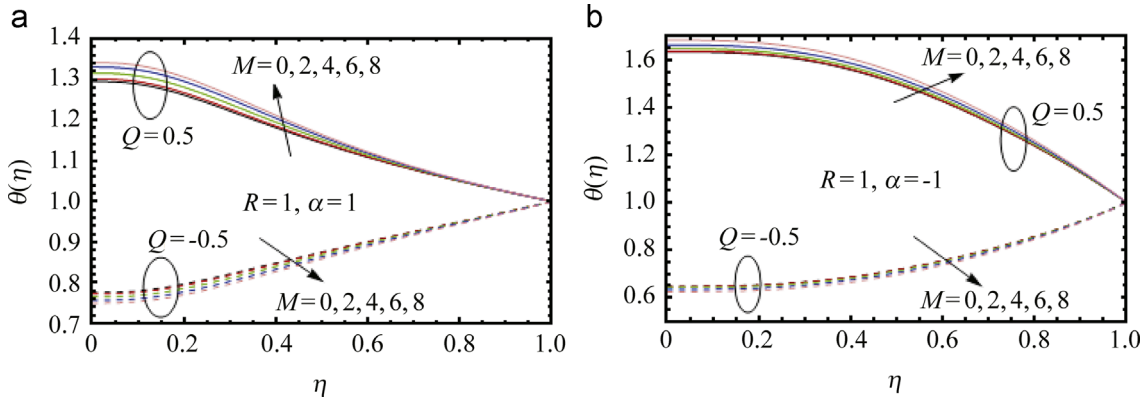

Figure 8 Effect of Hartmann number M on temperature distribution.

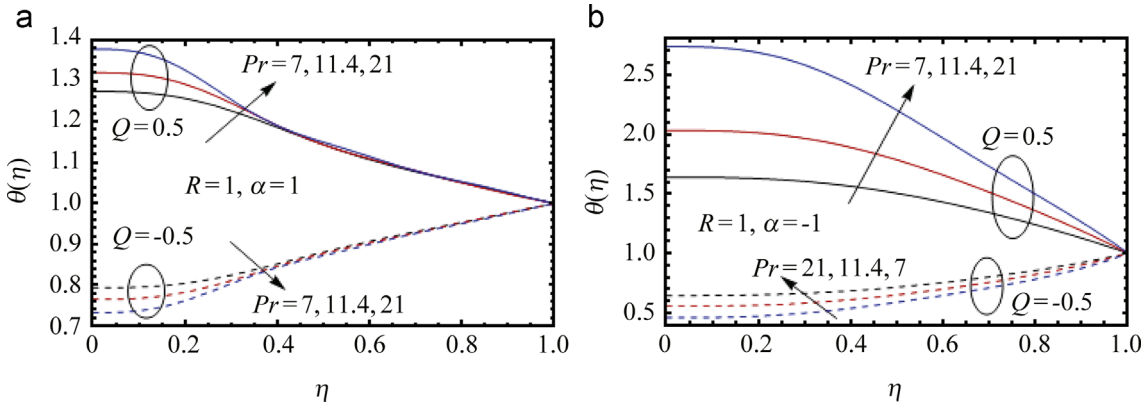

Figure 9 Effect of Prandtl number Pr on temperature distribution.

parameters Nb and Nt characterize the strengths of Brownian motion and thermophoresis effects. The larger values of Nb and Nt, the larger will be the strength of the corresponding effects. Thus Nb and Nt can take any value in the range of $0 \leq Nb, Nt < \infty$.

The effects of Brownian motion parameter, heat source or sink parameter, thermophoresis parameter, the wall expansion ratio, Hartmann number, Prandtl number and the permeation Reynolds number on the temperature field θ are shown in Figures 4–10. Figure 4(a) and (b) display the influence of Brownian motion parameter on the temperature profiles for both the cases of injection combined with wall expansion and contraction. It is observed that the temperature increases for both the cases of injection combined with wall expansion and contraction with an increase in Nb for $Q<0$. This is due to fact that an increase in the strength of Brownian motion leads to effective movement of nanoparticles from the wall to the fluid which results in the significant increase in θ. This opposite behavior is found for $Q>0$. The influence of heat source/sink parameter on the temperature for both the cases of injection combined with wall expansion and contraction is shown in Figure 5(a) and (b). As expected that heat source provides an increase in temperature for both the cases of injection combined with

wall expansion and contraction, while heat sink provides decrease in temperature. Figure 6(a) and (b) show the effect of thermophoresis parameter on the temperature for both the cases of injection combined with wall expansion and contraction. One can observe that θ increases for a given increase in Nt. Figure 7(a) and (b) depict the effect of wall expansion ratio on the temperature. For irrespective of suction or injection, θ increases as α increases in the presence of heat sink (i.e., $Q<0$) for the case of wall expansion, while it decreases as $|\alpha|$ increases for the case of wall contraction. But the behavior is reversed for the case of heat source (i.e., $Q>0$). Figure 8(a) and (b) illustrate the temperature profiles for different values of Hartmann number. It is observed that similar to common fluids, nanofluids show the same characteristics regarding Hartmann number on temperature. As increasing Hartmann number, the temperature increases in the presence of heat source for both the cases of wall expansion and contraction combined with injection. The opposite observation can be seen for the case of heat sink. Figure 9(a) and (b) elucidate the effect of the Prandtl number on θ. It is important note that the liquid metals and oils are characterized by the Prandtl number. The small values of Pr characterize the liquid metals which have high thermal conductivity and low

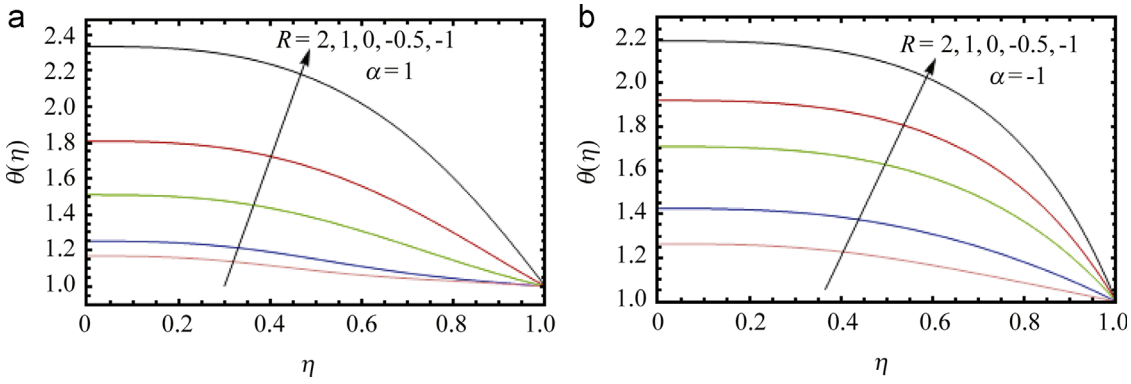

Figure 10 Effect of permeation Reynolds number R on temperature distribution.

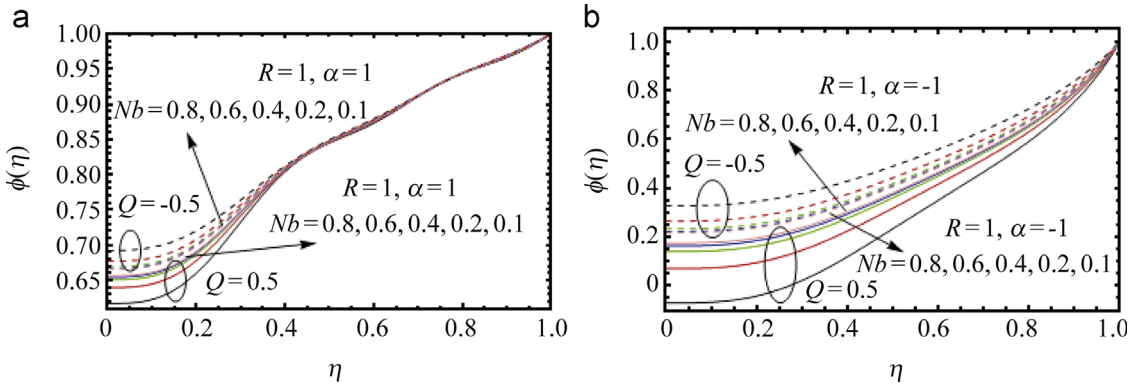

Figure 11 Effect of Nb on nanoparticle concentration distribution.

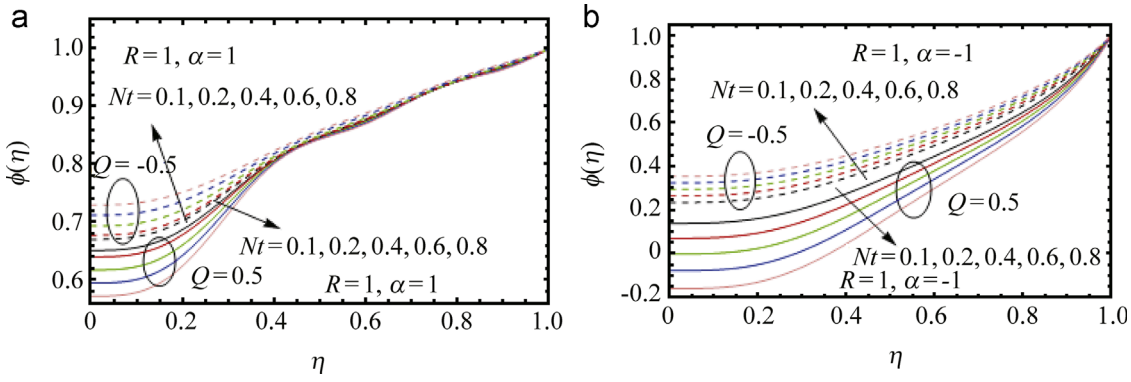

Figure 12 Effect of Nt on nanoparticle concentration distribution.

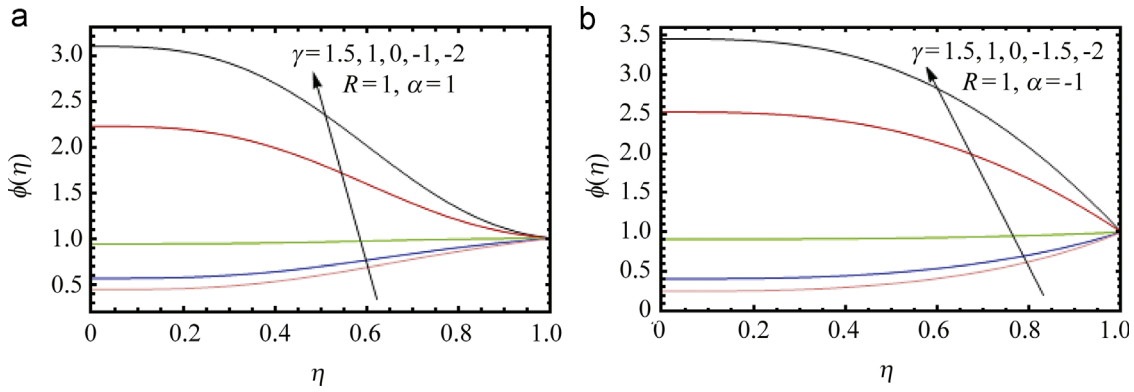

Figure 13 Effect of γ on nanoparticle concentration distribution.

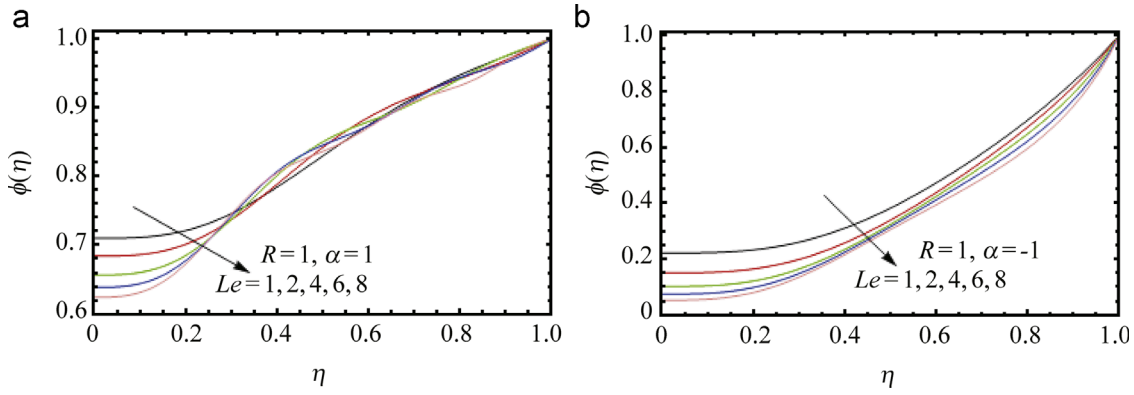

Figure 14 Effect of Le on nanoparticle concentration distribution.

viscosity, while larger values Pr correspond to high viscosity oils. Prandtl number $Pr = 7,\ 11.4,\ 21$ for water, water at 4 °C and human blood respectively. It is obvious that for both the cases of wall expansion and contraction combined with injection, the temperature decreases as Pr increases (i.e. increasing thermal diffusivity) in the presence of heat sink, while it increases for case of heat source. Figure 10(a) and (b) show the effect of permeation Reynolds number on the temperature. It is observed that for a given increase in injection the boundary layer thickness decreases and as a result θ decreases for both the cases of injection combined with wall expansion and contraction. The behavior is reversed for suction combined with wall expansion and contraction.

Figures 11–15 show the influence of Brownian motion parameter, thermophoresis parameter, chemical reaction parameter, Lewis number and wall expansion ratio on nanoparticles concentration. Figure 11(a) and (b) indicates that ϕ is a decreasing function of Nb in the presence of heat sink for both the cases of wall expansion and contraction combined with injection, while it is increasing function of Nb for the case of heat source. Figure 12(a) and (b) elucidates the effect of thermophoresis parameter on nanoparticle concentration. It is clear that in presence of heat sink, nanoparticle concentration increases with an increase in Nt for the both the cases of wall expansion and contraction combined with injection. From the physical point of view, an increase in thermophoresis parameter generates the larger mass flux due to temperature gradient which in turn raises the concentration. From the same figure, the opposite behavior can be observed in the presence of heat source. The effect of chemical reaction parameter which is positive for a destructive reaction and negative for a generative reaction on nanoparticle concentration is shown Figure 13(a) and (b). It is noticed that for the case of destructive chemical reaction parameter ($\gamma > 0$), for a given increase in γ, there is a decrease in nanoparticle concentration. Further, the behavior is reversed for the case of generative chemical reaction. Figure 14(a) and

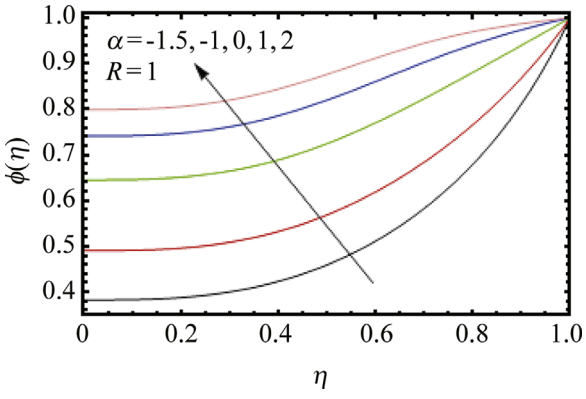

Figure 15 Effect of α nanoparticle concentration distribution.

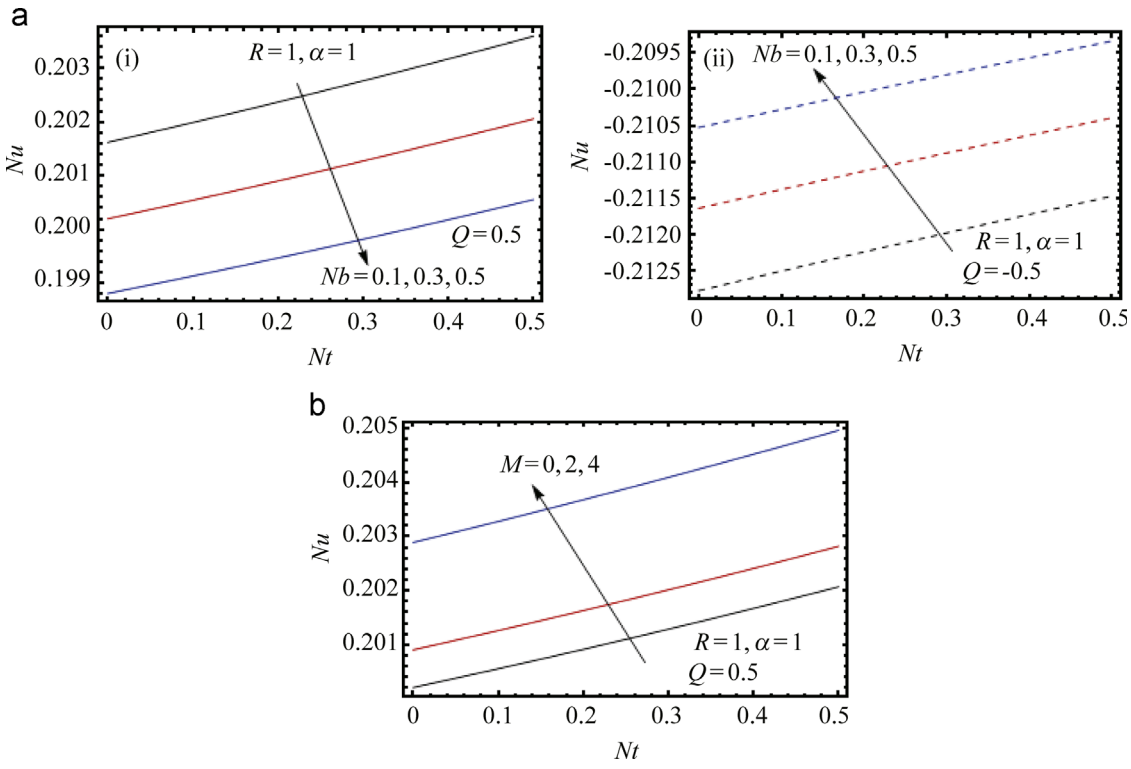

Figure 16 Nusselt number distribution.

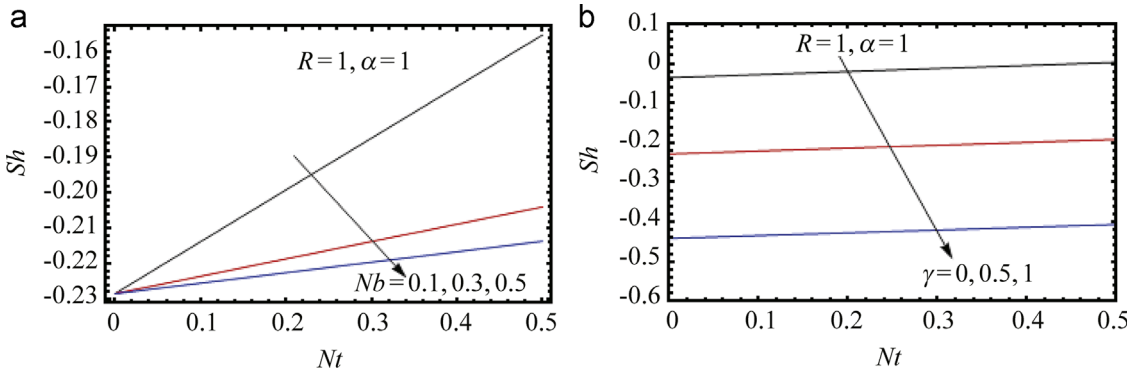

Figure 17 Sherwood number distribution.

(b) illustrate the effect of Lewis number Le on ϕ. One can observe that ϕ is a decreasing function of Le. This may be due to fact that increasing of Lewis number increases mass transfer rate and hence nanoparticle concentration decreases. Figure 15 shows the effect of wall expansion ratio α on ϕ. For irrespective of injection, nanoparticle concentration increases for a given increase in α, for the case of wall expansion, while it decreases as $|\alpha|$ increases for the case of wall contraction.

The effects of Brownian motion parameter and Hartmann number on Nusselt number Nu are shown in Figure 16 (a) and (b) respectively against thermophoresis parameter Nt. It is noticed that the Nusselt number is in proportion to Nt at the pipe wall. From Figure 16(a) it is clear that Nu increases as Nb increases at the wall for $Q<0$ (see Figure 16(aii)), while it decreases for $Q>0$ (see Figure 16(ai)). From Figure 16(b) it is noticed that Nu increases for a given increase in M at the wall. The influence of Brownian motion parameter and chemical reaction parameter on Sherwood number Sh is shown in Figure 17(a) and (b) against thermophoresis parameter. One can observe that the Sh increases with an increase in Nt at the wall. From Figure 17(a) it is clear that Sh decreases with an increase in Nb at the wall. From Figure 17(b) it is noticed that Sh decreases for a given increase in γ at the wall.

5. Conclusions

In this study we have examined the effects of chemical reaction and heat source/sink on MHD flow of nanofluid in

expanding or contracting porous pipe. The governing equations in cylindrical coordinates are introduced and transformed into a system of nonlinear ordinary differential equations using similarity transformations and then solved by employing HAM. The convergence of obtained series solutions is analyzed. The main findings are summarized as follows:

- It is observed that the temperature significantly increases with an increase in Brownian motion parameter, thermophoresis parameter for both the cases of wall expansion and contraction combined with injection.
- Heat source provides an increase in temperature for both the cases of injection combined with wall expansion and contraction, while heat sink provides decrease in temperature.
- The temperature increases with an increase in Hartmann number and Prandtl number for the case of heat source, while it decreases for the case of heat sink.
- In the presence of heat sink, nanoparticle concentration increases with an increase in Nt for the both the cases of wall expansion and contraction combined with injection.
- ϕ is a decreasing function of Nb in the presence of heat sink for both the cases of wall expansion and contraction combined with injection, while it increases for the case of heat source. Further, the nanoparticle concentration decreases for $\gamma > 0$ and increases for $\gamma < 0$.
- In the absence of nanoparticle concentration, the results of Srinivas et al. [13] for case the viscous fluid can be recovered by taking $Nb = Nt = Q = \gamma = 0$.

Acknowledgments

The authors gratefully acknowledge National Board for Higher Mathematics, India for sanctioning a major research project under the Grant no. 2/48(19)/2012/ NBHM(R.P.)/ R&D II/9137. The authors thank all the three anonymous reviewers for their constructive comments and suggestions.

References

[1] S. Uchida, H. Aoki, Unsteady flows in a semi-infinite contracting or expanding pipe, J. Fluid Mech. 82 (1977) 371–387.
[2] M. Goto, S. Uchida, Unsteady flows in a semi-infinite contracting or expanding pipe with a porous wall, Theor. Appl. Mech. 40 (1991) 161–172.
[3] J. Majdalani, C. Zhou, Moderate-to-large injection and suction driven channel flows with expanding or contracting walls, Z. Angew. Math. Mech. 83 (2003) 181–196.
[4] X. Si, L. Zheng, X. Zhang, Y. Chao, Perturbation solution to unsteady flow in a porous channel with expanding or contracting walls of a transverse magnetic field, Appl. Math. Mech. 31 (2010) 151–158.
[5] J. Majdalani, G.L. Flandro, The oscillatory pipe flow with arbitrary injection, Proc. R. Soc. Lond. A 458 (2002) 1621–1651.
[6] J. Majdalani, C. Zhou, C.A. Dawson, Two-dimensional viscous flow between slowly expanding or contracting walls with weak permeability, J. Biomech. 35 (2002) 1399–1403.
[7] R.M. Terrill, P.W. Thomas, Spiral flow in a porous pipe, Phys. Fluids 16 (1973) 356–359.
[8] E.C. Dauenhauer J. Majdalani, Unsteady flows in semi-infinite expanding channels with wall injection, AIAA Paper, 99-3523, 1999.
[9] Y.Z. Boutros, M.B. Abd-el-Malek, N.A. Badran, H.S. Hassan, Lie-group method for unsteady flows in a semi-infinite expanding or contracting pipe with injection or suction through a porous wall, J. Comput. Appl. Math. 197 (2006) 465–494.
[10] X.H. Si, L.C. Zheng, X.X. Zhang, M. Li, J.H. Yang, Y. Chao, Multiple solutions for the laminar flow in a porous pipe with suction at slowly expanding or contracting wall, Appl. Math. Comput. 218 (2011) 3515–3521.
[11] S. Asghar, M. Mushtaq, T. Hayat, Flow in a slowly deforming channel with weak permeability: An analytical approach, Nonlinear Anal.: Real World Appl. 11 (2010) 555–561.
[12] S. Srinivas, A. Subramanyam Reddy, T.R. Ramamohan, A study on thermal-diffusion and diffusion-thermo effects in a two-dimensional viscous flow between slowly expanding or contracting walls with weak permeability, Int. J. Heat Mass Transf. 55 (2012) 3008–3020.
[13] S. Srinivas, A. Subramanyam Reddy, T.R. Ramamohan, A. K. Shukla, Influence of heat transfer on MHD flow in a pipe with expanding or contracting permeable wall, Ain Shams Eng. J. 5 (2014) 817–830.
[14] S.U.S. Choi, Enhancing thermal conductivity of fluids with nanoparticle, in: D.A. Siginer, H.P. Wang (Eds.), Developments and Applications of Non-Newtonian Flows, FED-V.231/MD-V.66, ASME, New York, USA, 1995, pp. 99–105.
[15] X.Q. Wang, A.S. Mujumdar, A review on nanofluids, part I: theoretical and numerical investigations, Braz. J. Chem. Eng. 25 (2008) 613–630.
[16] S.U.S. Choi, Nanofluids: a new field of scientific research and innovative applications, Heat Transf. Eng. 29 (2008) 429–431.
[17] W.A. Khan, I. Pop, Boundary-layer flow of a nanofluid past a stretching sheet, Int. J. Heat Mass Transf. 53 (2010) 2477–2483.
[18] O.D. Makinde, A. Aziz, A boundary layer flow of a nanofluid past a stretching sheet with convective boundary conditions, Int. J. Therm. Sci. 50 (2011) 1326–1332.
[19] M. Sheikholeslami, M. Hatami, D.D. Ganji, Analytical investigation of MHD nanofluid flow in a semi-porous channel, Powder Technol. 246 (2013) 327–336.
[20] M. Mustafa, S. Hina, T. Hayat, S. Alsaedi, Influence of wall properties on the peristaltic flow of a nanofluid: analytical and numerical solutions, Int. J. Heat Mass Transf. 55 (2012) 4871–4877.
[21] J. Buongiorno, Convective heat transport in nanofluids, J. Heat Transf. 128 (2006) 240–250.
[22] N.C. Rosca, I. Pop, Unsteady boundary layer flow of a nanofluid past a moving surface in an external uniform free stream using Buongiorno's model, Comput. Fluids 95 (2014) 49–55.
[23] A.V. Kuznetsov, D.A. Nield, Natural convective boundary-layer flow of a nanofluid past a vertical plate, Int. J. Therm. Sci. 49 (2010) 243–247.
[24] S. Nadeem, R. Mehmood, N.S. Akbar, Non-orthogonal stagnation point flow of a nano non-Newtonian fluid towards

a stretching surface with heat transfer, Int. J. Heat Mass Transf. 57 (2013) 679–689.
[25] H. Xu, I. Pop, Fully developed mixed convection flow in a vertical channel filled with nanofluids, Int. Commun. Heat Mass Transf. 39 (2012) 1086–1092.
[26] M. Mustafa, M. Nawaz, T. Hayat, A. Alsaedi, MHD boundary layer flow of second grade nanofluid over a stretching sheet with convective boundary conditions, J. Aerosp. Eng. 27 (2014) 1–7.
[27] A. Alsaedi, M. Awais, T. Hayat, Effect of heat generation/absorption on stagnation point flow of nanofluid over a surface with convective boundary conditions, Commun. Nonlinear Sci. Numer. Simul. 17 (2012) 4210–4223.
[28] J. Chamkha, A.M. Rashad, A.M. Aly, Transient natural convection flow of a nanofluid over a vertical cylinder, Meccanica 48 (2013) 71–81.
[29] A. Malvandi, S.A. Moshizi, E.G. Soltani, D.D. Ganji, Modified Buongiorno's model for fully developed mixed convection flow of nanofluids in a vertical annular pipe, Comput. Fluids 89 (2014) 124–132.
[30] M. Akbari, A. Behzadmehr, F. Shahraki, Fully developed mixed convection inhorizontal and inclined tubes with uniform heat flux using nanofluid, Int. J. Heat Fluid Flow 29 (2008) 545–556.
[31] R. Ellahi, The effects of MHD and temperature dependent viscosity on the flow of non-Newtonian nanofluid in a pipe: analytical solutions, Appl. Math. Model. 37 (2013) 1451–1467.
[32] M.J. Uddin, O.A. Beg, N. Amin, Hydromagnetic transport phenomena from a stretching or shrinking nonlinear nanomaterial sheet with Navier slip and convective heating: a model for bio-nano-materials processing, J. Magn. Magn. Mater. 368 (2014) 252–261.
[33] H. Xu, T. Fan, I. Pop, Analysis of mixed convection flow of a nanofluid in vertical a channel with Buongiorno mathematical model, Int. Commun. Heat Mass Transf. 44 (2013) 15–22.
[34] M.Y. Malik, M. Naseer, S. Nadeem, A. Rehman, The boundary layer flow of Casson nanofluid over a vertical exponentially stretching cylinder, Appl. Nanosci. 4 (2014) 869–873.
[35] A. Malvandi, D.D. Ganji, Brownian motion and thermophoresis effects on slip flow of alumina/water nanofluid inside a circular micro channel in the presence of a magnetic field, Int. J. Therm. Sci. 84 (2014) 196–206.
[36] K. Zaimi, A. Ishak, I. Pop, Unsteady flow due to a contracting cylinder in a nanofluid using Buongiorno's model, Int. J. Heat Mass Transf. 68 (2014) 509–513.
[37] S. Srinivas, A. Vijayalakshmi, T.R. Ramamohan, A. Subramanyam Reddy, Hydromagnetic flow of a nanofluid in a porous channel with expanding or contracting walls, J. Porous Media 17 (2014) 953–967.
[38] F. Hedayati, G. Domairry, Effects of nanoparticle migration and asymmetric heating on mixed convection of TiO_2-H_2O nanofluid inside a vertical micro channel, Powder Technol. 272 (2015) 250–259.
[39] A. Malvandi, M.R. Safaei, M.H. Kaffash, D.D. Ganji, MHD mixed convection in a vertical annulus filled with Al_2O_3-water nanofluid considering nanoparticle migration, J. Magn. Magn. Mater. 382 (2015) 296–306.
[40] K. Vajravelu, K.V. Prasad, N.S.P. Rao, Diffusion of a chemically reactive species of a power-law fluid past a stretching surface, Comput. Math. Appl. 62 (2011) 93–108.
[41] R. Cortell, MHD flow and mass transfer of an electrically conducting fluid of a second grade in a porous medium over a stretching sheet with chemically reactive species, Chem. Eng. Process.: Process Intensif. 46 (2007) 721–728.
[42] C. Bridges, K.R. Rajagopal, Pulsatile flow of a chemically-reacting nonlinear fluid, Comput. Math. Appl. 52 (2006) 1131–1144.
[43] S. Nadeem, N.S. Akbar, Influence of heat and chemical reactions on Walter's B fluid model for blood flow through a tapered artery, J. Taiwan Inst. Chem. Eng. 42 (2011) 67–75.
[44] T. Hayat, Z. Abbas, Channel flow of a Maxwell fluid with chemical reaction, Z. Angew. Math. Phys. 59 (2008) 124–144.
[45] R. Abdul-Kahar, R. Kandasamy, Muhaimin, Scaling group transformation for boundary-layer flow of a nanofluid past a porous vertical streching surface in the presence of chemical reaction with heat radiation, Comput. Fluids 52 (2011) 15–21.
[46] P.K. Kameswaran, S. Shaw, P. Sibanda, P.V.S.N. Murthy, Homogeneous–heterogeneous reactions in a nanofluid due to a porous stretching sheet, Int. J. Heat Mass Transf. 57 (2013) 465–472.
[47] M.J. Uddin, W.A. Khan, A.I. Ismail, Lie group analysis and numerical solutions for magneto convective slip flow along a moving chemically reacting radiating plate in porous media with variable mass diffusivity, Heat Transf.-Asian Res. (2014), http://dx.doi.org/10.1002/htj.21161.
[48] M.M. Rashidi, E. Momoniat, M. Ferdows, A. Basiriparsa, Lie group solution for free convective flow of a nanofluid past a chemically reacting horizontal plate in porous media, Math. Probl. Eng. 2014 (2014) 1–21.
[49] S. Srinivas, A. Subramanyam Reddy, T.R. Ramamohan, Mass transfer effects on viscous flow in an expanding or contracting porous pipe with chemical reaction, Heat Transf.-Asian Res. 44 (2015) 552–567.
[50] M.J. Uddin, O.A. Beg, A. Aziz, A.I.M. Ismail, Group analysis of free convection flow of a magnetic nanofluid with chemical reaction, Math. Probl. Eng. 2015 (2015) 1–11.
[51] S.J. Liao, Beyond Perturbation: Introduction to Homotopy Analysis Method, CRC Press, Chapman and Hall, Boca Raton, 2003.
[52] S.J. Liao, Advances in the homotopy analysis method, World Sci. (2014).
[53] X. Hang, Z.L. Lin, S.J. Liao, J. Majdalani, Homotopy based solutions of the Navier–Stokes equations for a porous channel with orthogonally moving walls, Phys. Fluids 22 (2010) 053601-18.
[54] M. Turkyilmazoglu, Purely analytic solutions of magnetohydrodynamic swirling boundary layer flow over a rotating porous disk, Comput. Fluids 39 (2010) 793–799.
[55] S. Xinhui, L. Zheng, P. Lin, X. Zhang, Y. Zhang, Flow and heat mass trasfer of a micropolar fluid in a porous channel with expanding or contracting walls, Int. J. Heat Mass Transf. 67 (2013) 885–895.
[56] S. Srinivas, A. Gupta, S. Gulati, A. Subramanyam Reddy, Flow and mass transfer effects on viscous fluid in a porous channel with moving/stationary walls in presence of chemical reaction, Int. Commun. Heat Mass Transf. 48 (2013) 34–39.
[57] T. Hayat, R. Naz, S. Abbasbandy, On flow of a fourth grade fluid with heat transfer, Int. J. Numer. Methods Fluids 67 (2011) 2043–2053.